An analysis of thixotropic micropore variation and its mechanism in loess

Le Wei[1], Faning Dang[1]*, Jiulong Ding[1], Xiaojuan Wu[1], Jiayang Li[1] and Zhengzheng Cao[2]*

[1]Xi'an Key Laboratory of Environmental Geotechnical Engineering of Loess Plateau, Xi'an University of Technology, Xi'an, China, [2]School of Civil Engineering, Henan Polytechnic University, Jiaozuo, Henan, China

The relationship between the thixotropic mechanism and the macroscopic thixotropic strength can be clarified by analyzing the changes in microstructure and pores in the loess thixotropic process. This approach is of significant importance for calculating the strength of compacted loess foundations. In the present study, a representative sample prepared from Xi'an loess was analyzed and eight resting ages were set. The micropore characteristics of the remolded loess and undisturbed loess at different resting ages were obtained using electron microscope observation and nuclear magnetic resonance testing. The results indicate that the thixotropy in the prepared loess samples is significant. It is also found that as the resting age grew, newly formed cements in the remolded loess continuously accumulated and filled in the microcracks between the aggregates. Consequently, the contact area of aggregates increased, thereby decreasing the width and length of the microcracks. The proportion of cementation pore and small microcracks gradually increased, while the proportion of large microcracks gradually decreased, indicating that thixotropy increased the cohesive force and friction force of soil structure at the mesoscale. This phenomenon also explains the increase of thixotropic strength at the macroscopic scale. The mesoscopic mechanism of loess thixotropic strength recovery is that the connection between soil particles is re-established after the break of the clay particle−water−charge system. Moreover, the elastic potential energy of soil particles generated by compression promoted the polymerization of clay particles dispersed in a pore water solution to produce flocculating aggregates during resting dissipation. The continuous consumption of clay particles expanded the processing time and flocs and continuously decreased the strength growth rate.

KEYWORDS

loess, thixotropy, microscopic, microcrack, cementation

1 Introduction

Geological surveys indicate the widespread presence of large and thick loess strata in northern China. With the rapid economic development in the past few decades, numerous construction activities are under process on these loess foundations. Furthermore, recent economic developments have led to the rapid expansion of most cities. It is worth noting that some cities are located in loess gully mountain areas, wherein conducting mountain

digging and trench-filling projects is an enormous challenge to provide space for expansion. The excavated area in the loess foundation consists of undisturbed loess that has undergone millions of years of natural deposition. As a result, the strength of the loess foundation is typically high and stable. This allows for an accurate assessment of the bearing capacity of the foundation, ensuring the safety and stability of construction projects conducted in the area. However, the excavated area has a remolded loess foundation so its strength is far lower than that of the undisturbed loess foundation even after rolling and ramming processes, which are typically carried out to compact the area. Moreover, an area with a large fill thickness usually has long-term post-construction settlement, which is generally shelved for many years. Some underground space projects with lower loads may be constructed, such as underground warehouses or energy storage facilities (Xue et al., 2023a; Xue et al., 2023b). During the shelving of the foundation, while the soil settles and deforms, various coupling effects such as soil water pressure and geothermal energy can also occur, affecting the strength of the foundation soil (Liu et al., 2023; Yang et al., 2023). These coupling effects also affect the structural stability of underground space engineering during shelving (Jiang et al., 2022; Xue et al., 2023c). During the period of foundation shelving, the bearing capacity of the foundation increases continuously. This may be attributed to two primary reasons: creep consolidation and thixotropy of loess. Creep consolidation refers to the long-term compaction of loess, leading to an increase in the strength of the soil structure. Thixotropy, on the other hand, relates to the strengthening of chemical composition cementation within the soil structure when the soil body does not change. While there have been numerous studies on the consolidation of loess, further investigations are needed to better understand the thixotropy of loess.

The term "thixotropy" was initially coined by Peterfi (1927) to describe the interconversion of colloidal solutions between fluid and elastic solids. Since then, the concept of thixotropy has been widely used in the field of geotechnical materials to describe the gradual increase in soil strength over time after reshaping disturbance by Burgers and Blair (1949). Boswell (1948) conducted a study on thixotropic materials in various soils and found that except for pure sand lacking fine particles, geotechnical materials exhibit different degrees of thixotropy. A review of the literature reveals that the internal mechanism of the thixotropic process has been extensively analyzed. For example, Mitchell (1961) conducted experiments and demonstrated that the thixotropic effect of the soil–water mixture on the spacing of soil particles is much greater than that of chemical composition. Zhang et al. (2017) studied the thixotropy of Zhanjiang soft clay and indicated that variations in the internal force field of the soil affect the pore structure between particles, thereby affecting the strength of the soil over the resting ages. Day (1954) carried out experimental investigations and revealed that when the soil is disturbed, the internal energy and stress state of the structure changes over time. Accordingly, Mitchell (1961) proposed a new theoretical hypothesis for soil thixotropy, pointing out that thixotropy is a structural effect that relates to the arrangement of soil

particles, pore water distribution, and ion content. Furthermore, it was found that energy within the structure consistently dissipates during thixotropy. Díaz-Rodríguez and Santamarina (1999) indicated that the essential thixotropy mechanism originates from changes in the internal energy of soil, chemical reactions between minerals, mechanical loads, and transmission of electrons within the microstructure. Blake and Gilman (1970) and Rinaldi and Clari´a (2016) indicated that when soil is disturbed, chemical bonds between particles are broken and the system enters a dispersed state. In this case, the repulsive force between soil particles exceeds the gravitational force, and the internal energy slightly strengthens. As energy is partially dissipated and the gravitational force surpasses the repulsive force, the energy level of the soil–water–electric system decreases, and dispersed particles fluctuate in the soil.

The thixotropic model has been gradually proposed and applied to calculate the strength of rock and soil materials. Dexter et al. (1988) proposed a simplified thixotropic model of the number of bonds between soil particles over time. At a resting age of 0d, the soil failure strength is related to the force and the corresponding failure surface area when the bond number between particles is broken. At the resting ages t, the structure strength is enhanced by the formation of new bonds between soil particles due to thixotropy, and the formation of new bonds is independent of compaction. Doglioni and Simeone (2013) pointed out that when soil is subjected to high effective stress, the position and shape of soil particles are not easy to change due to the restriction of neighboring particles. Heymann et al. (1996) proposed another model of thixotropic behavior change related to yield strength change, pointing out that thixotropic strength is an exponential function related to different material properties. Abu-Farsakh et al. (2015) introduced a time-dependent reduction parameter β into the thiotropic strength calculation formula proposed by Heymanneq, it is introduced into the finite element model to simulate the increase of soil thixotropic strength around the pile before and after thixotropic change. The calculated results are close to those of the instrument pile load test. In addition, some scholars have studied the thixotropy of geotechnical materials by using thixotropy models such as viscosity, viscoelasticity or viscoplasticity of suspension or gel (Barnes, 1997; Dullaert and Mewis, 2006; de Souza Mendes, 2009).

The thixotropic theory has been verified using advanced testing techniques. In this regard, Zhang et al. (2017) evaluated this theory by studying the microscopic thixotropy mechanism in Zhanjiang soft clay using electron microscopy observation and mercury injection tests. Osipov et al. (1984) utilized a rotating viscometer, analyzed changes in the microstructure of thixotropic soil before and after vibration, and indicated that relatively uniform and dispersed micro-cracks form in the soil during vibration. It was found that when the soil is under vibration, the size of micro-aggregates gradually increases over time, the pore size increases and the soil structure develops to the initial state. Jacobsson and Pusch (1972) studied the thixotropy of quick-clays using transmission electron microscopy, microsection, and nuclear spin echo. It was found that thixotropic structure recovery is related to the

reorientation of small particles and changes in pore water solution. Aminpour (2019) performed numerical simulations based on multifunctional molecular dynamics, explored the interaction between soil particles over time, and clarified the relationship between clay thixotropy at the macro- and micro-levels. Although significant progress has been made in understanding the microscopic characteristics of thixotropic, the existing technologies have some shortcomings. For example, scanning electron microscopy (SEM) may not accurately capture the exact location of the sample, and the mercury injection pore method can damage the sample structure. To address these challenges, environmental scanning electron microscopy (ESEM) and computed tomography (CT) were proposed (Gagnoud et al., 2008; Pardo et al., 2019; Sun et al., 2019; Sun et al., 2020).

The relationship between mineral composition and thixotropic micromechanical properties of soil has also been explored extensively. Skempton and Northey (1952) studied the thixotropy of different clay minerals and found that bentonite exhibits the most pronounced structural change in a short time. This may be attributed to the high thixotropy nature of bentonite, while Illite has low thixotropy and kaolin has almost no thixotropy. Similar results were also obtained by Shahriar et al. (2018). Jeong et al. (2012) conducted experiments and found that higher soil activity corresponds to more prominent thixotropy. Furthermore, Shahriar et al. (2018) carried out thixotropic mechanical tests on six types of clay and found that the stronger the soil activity at resting ages of 1d and 8d, the greater the thixotropic-induced increases in strength. Abdou and Ahmed (2013) demonstrated that the thixotropic degree is positively correlated with soil activity by adjusting the bentonite content. Andersen et al. (2008) analyzed the thixotropic test data and revealed a correlation between the strength and activity level of the soil. Zhang et al. (2017) carried out experiments and demonstrated that highly active minerals have a larger specific surface area, which can increase more cationic exchange capacity and charge quantity to enhance thixotropy.

Additionally, the effect of salt concentration of pore water on the degree of thixotropy has been explored in detail. In this context, Jeong et al. (2012) studied the relationship between salt concentration and thixotropy in clay with high montmorillonite content and revealed that salt concentration significantly affects yield stress and plastic viscosity. Lu et al. (1991) found that soil samples made with fresh water exhibit slightly higher thixotropic strength compared to those made with salt water. Perret et al. (1996) prepared mud samples with different salt concentrations ranging from 0.1 to 30 g/L and found that samples with low salinity exhibit higher thixotropy. Similarly, Abdou and Ahmed (2013) prepared bentonite mud samples with different salt concentrations and found that low salt concentration results in high thixotropy, while high salt concentration leads to almost no thixotropy. Olphen (1977) demonstrated that high salt concentration in pore water may change the thickness of the double electric layer between soil particles, thereby reducing the interaction attraction between soil particles, and reducing the thixotropy. Perret et al. (1996) carried out experiments and indicated that when the salt concentration is low, the bond energy between soil particles is strong. This phenomenon induces flocculation, thereby increasing the thixotropy degree.

The performed literature survey highlights a gap in the research on thixotropy specifically in loess samples. Most studies have focused on clay and mud samples, while there are limited in-depth investigations on the thixotropy behavior of loess. Moreover, studies on the thixotropic mechanism have prominently explored the micro level and the relationship between soil particles has been analyzed extensively. However, the transition relationship of thixotropy from micro-scale to macro-mechanical strength improvement cannot theoretically support the calculation of the bearing capacity of the remolded loess foundation, and further investigation is required in this area. Aiming at resolving these shortcomings, the present study utilized the electron microscopy technique to observe the mesoscopic void changes of the undisturbed and remolded loess of different resting ages at low multiples. Moreover, nuclear magnetic resonance technology was used to observe the aperture distribution proportions of the undisturbed and remolded loess of different resting ages at different scales to analyze the relationship between the thixotropy of loess and the changes in mesoscopic pores. The main objective of this article was to clarify the thixotropic mechanism of loess at mesoscopic scales. The results are expected to provide a basis for further understanding of the growth of macro-scale strength. Meanwhile, it is intended to propose an expression for the growth of macro-scale strength caused by the thixotropy-induced changes in the mesostructure of loess.

2 Test samples and the analysis method

2.1 Test soil sample

The test samples were prepared from a construction site 1km north of the North Wall of Weiyang District, Xi'an, Shaanxi Province, China. It was Q_2 loess with a depth of 10–12m. The physical properties of the soil sample are presented in Table 1, the chemical composition and classification of the soil sample particles are presented in Table 2, the concentration of different cements in the soil sample (%) are presented in Table 3.

2.2 Test methods and sample preparation

To study the relationship between the microstructural changes and the macroscopic thixotropic strength of loess during the thixotropic process and analyze the variations in the microstructural mechanism of the thixotropic strength, the microstructure of the undisturbed and remolded loess samples was analyzed after resting for 0d, 5d, 10d, 20d, 40d, 80d, 120d, and 160d. Electron microscopy (SEM) was utilized to observe the soil structure and pore morphology at different scales, and nuclear magnetic resonance (NMR) was used to measure the aperture distribution ratio in the soil.

TABLE 1 Basic physical properties of loess in Xi'an.

Natural water content(%)	Natural density (g/cm³)	Relative density	Porosity	Plastic limit/ W_p(%)	Liquid limit/ W_L(%)	Plastic index$_{Ip}$
25.4	1.73	2.71	0.49	19.4	30.8	11.4

2.2.1 Preparation of the remolded samples at different resting ages

The loose soil sample is configured as the soil sample with the same water content as the undisturbed soil sample, and the dry density of the sample is the same as that of the undisturbed soil by using a triaxial standard compactor. After demoulding, it is sealed with plastic wrap and tin foil to prevent water evaporation. After resting different test ages, it is made into electron microscope observation sample or nuclear magnetic resonance test sample.

2.2.2 Observation of mesoscopic pore structure of soil

The configuration of scanning electron microscope equipment is illustrated in Figure 1. To conduct analyses, standard triaxial samples with a diameter of 3.91cm and a height of 8cm were prepared from the undisturbed and remolded soil samples of different resting ages. After drying the samples in an oven, the soil around the cylindrical side was removed to ensure that the structure of the selected samples is intact. The section size of the remaining central position is about a strip of soil with a side length of 1cm. The section was extracted as shown in Figure 2. After dust removal, the fresh section was put into the electron microscope lofting box for observation.

2.2.3 Calculation of soil pore proportion at different scales

The principle of nuclear magnetic resonance (NMR, MesoMR23-060H-1 Suzhou Niumai Analytical Instrument, China) technology is to obtain the distribution spectrum of longitudinal signal strength and transverse relaxation time T_2 by measuring the relaxation characteristics of hydrogen ions in soil pore water. Then the distribution proportion of pores at different scales can be obtained through conversion. The conversion expression is as follows:

$$\frac{1}{T_2} \approx \rho_2 \left(\frac{2}{R} \right), \tag{1}$$

Where ρ_2 represents the surface relaxation strength, which is dependent on the material properties; R is the pore radius; the area enclosed by the T_2 spectral curve and the relaxation time of the abscissa is the total pore water content.

The configuration of the NMR device is shown in Figure 3. To conduct tests, standard triaxial samples with a diameter of 3.91 cm and a height of 8 cm were prepared. The prepared samples were wrapped with a hard plastic shell as shown in Figure 4 to prevent deformation of the saturated soil sample and change its structure during the test process. The outside of the hard plastic shell was sealed with tape, then packed with a saturator and vacuumed. When the saturation exceeded 95%, the saturator was removed, and the upper and lower ends of the sample were sealed with a plastic wrap to prevent test errors caused by the outflow of pore water inside the soil sample during the test process. The sample seal is illustrated in Figure 5.

During the resting process of the soil sample, thixotropy causes the accumulation of clay minerals inside the structure to produce flocs, thus increasing the strength. In this process, the water content of the soil remains unchanged, so the flocs belong to water-resistant collection. The soil samples observed by electron microscopy mainly produce dehydration consolidation after drying, and the saturated soil samples tested by nuclear magnetic resonance only affect the soluble and medium soluble substances in the soil, so the drying and water saturation effects are not easy to destroy the water-resistant insoluble substances produced by thixotropy.

3 Micropore changes during loess thixotropy

3.1 Observation of microstructure and pore changes in loess

In order to study the changes in the microstructure of loess during thixotropy and its correlation with the macroscopic thixotropy intensity, and explore the microstructure mechanism of the strength changes, the prepared samples were tested under various magnification rates. The results with a magnification of 300, 500, and 1000 times are shown in Figures 6, 7, 8, respectively. The development trend of overhead through macropores between large aggregates of soil samples at different resting ages can be obtained by 300 times observation. The change of cementation degree between small particles and the development trend of aperture in

TABLE 2 Composition and classification of loess particles.

Mass fraction of different particle sizes/%			Classify	
>0.075 mm	0.075~0.005 mm	<0.005 mm	Classified by plastic diagram	Classified by particle composition
12.5	63.2	24.3	CL	clay

TABLE 3 Concentration of different cements in loess (%).

Illite	Smectite	Kaolinite	Eutectic salt	Cation exchange capacity (mg/kg)	Free oxide	Organic matter
25.9	2.9	2.3	0.11	0.824	2.72	0.29

the soil macropore at different resting ages can be obtained by 500 times observation. The change of internal cementation degree and the development trend of aperture in the soil micropore at different resting ages can be obtained by 1000 times observation.

Figures 6A–I with a magnification of 300 times indicate that the remolded loess at different resting ages aggregates overhead and there is a small contact area between aggregates. Moreover, the overhead pores with an average size larger than 700 μm are in a state of through-development. The aperture is longer in the three-dimensional space, and no significant change in pore structure is observed as the resting ages grows. The undisturbed loess has a closed macropore structure with the aperture of approximately 600 μm. In this case, the overhead aggregation is relatively low, and the clay particles are closely consolidated with fine silt particles. It is observed that compared with the undisturbed loess, remolded loess with the same dry density and water content has the same porosity, but the macropore size of remolded loess is larger than that of undisturbed loess. Moreover, the consolidated area between the aggregates of the remolded loess is much smaller than that of the undisturbed loess, which decreases the strength of the remolded loess.

Figures 7A–I with a magnification of 500 times reveal the presence of 50–100 μm contact cementation regions between the aggregates of 100–300 μm in the remolded loess at different resting ages. It is also observed that as the resting ages grows, the cementation regions between the aggregates gradually increase and the regions

may even merge with each other. The length of the microcrack decreases or its width narrows, ultimately leading to the crack closure. This phenomenon may be attributed to the accumulation of newly generated clay cements in the crack due to thixotropy after soil resting. This phenomenon reduces the porosity connectivity at this size to a certain extent and increases the cohesion and friction between aggregates, which promotes the growth of the overall structural strength. In contrast, the undisturbed loess primarily contains closed pores, and there are almost no micro-cracks with loose cementation between aggregates.

Figures 8A–I show the results with a magnification of 1000 times, indicating that the remolded loess contains numerous small particles with sizes ranging from 20–50 μm. It is observed that as the resting ages increases, the degree of cementation among these small particles progressively intensifies, forming larger particles. In this case, the soil particles on the broken surface can be hardly peeled off by shear loads. Consequently, the occlusion between soil particles strengthens, enhancing the overall friction within the structure. In contrast, the undisturbed loess exhibits complete cementation among soil particles, and no loose tiny particle is observed in the undisturbed loess.

The observations of loess microstructure at different magnifications indicate that as the resting ages increases, the degree of cementation among the dispersed small aggregates (20–50 μm) within large aggregates increases, and the reinforced large aggregates enhance the
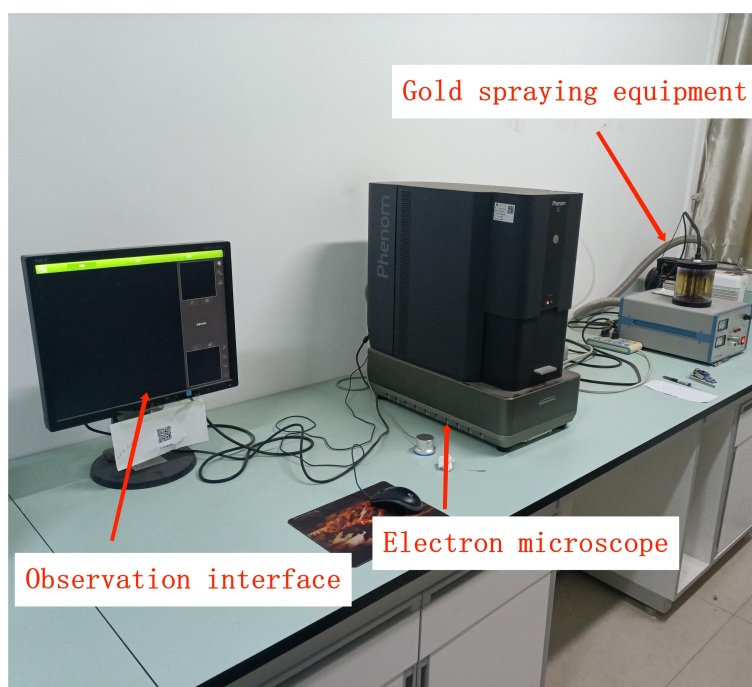

FIGURE 1
Electron microscope equipment.

FIGURE 2
Soil sample observation section.

friction force of the soil. Moreover, the newly formed cements accumulate between larger aggregates, resulting in the reduction of the microcrack lengths, narrowing the crack widths, or even the closure of microcracks. Cementing contact areas of 50–100 μm gradually develop between the aggregates of 100–300 μm, thereby increasing the cohesiveness and friction between the aggregates. These two effects increase the macroscopic structural strength of the soil.

3.2 Analysis of aperture distribution ratio at different scales in loess

3.2.1 T_2 spectrum and aperture distribution ratio curve conversion

The relationship between NMR relaxation time T_2 and the signal strength is illustrated in Figure 9. It is observed that the relaxation time is directly proportional to aperture in soil. The smaller the relaxation time T_2, the smaller the aperture. Meanwhile, the lower the relaxation signal intensity, the smaller the proportion of the pore content in the total pore.

3.2.2 Pore division and thixotropic proportion calculation

In the aperture distribution ratio curve, a certain aperture is set as r_a, aperture 0 to r_a is the micropore, and the other aperture is set

as r_b, r_b to 4000 μm is the macropore, r_a to r_b is the mesopore. The division of different pore interval is depicted in Figure 10 and Figure 11. In Figure 9, it is easy to know that the ratio of aperture distribution of remodeled loess corresponding to r_b is about 0, so r_b is approximately 400 μm. To determine r_a, it is defined that the pore segment with the increase of aperture distribution ratio with the increase of resting ages is the micropore segment, and the pore segment with the decrease of aperture distribution ratio is the mesopore segment. The peak value of aperture distribution ratio in the micropore segments at different resting ages is translated to the same peak value as that of soil samples at a resting age of 0d, so that the corresponding horizontal coordinate aperture is the same. It can be found in the figure that the aperture distribution ratio of the remolded soil samples under different resting ages overlaps around a small aperture interval. The aperture distribution ratio on the left side of the coincidence interval increases, while the aperture distribution ratio on the right side of the coincidence interval decreases. The minimum floating value of the coincidence interval is selected, and the corresponding aperture is about 7 μm. Therefore, it is determined that the micropore is 0–7 μm, the mesopore is 7–400 μm, and the macropore is 400–4000 μm.

It is known that the area enclosed by the aperture distribution ratio curve and the horizontal aperture represents the number of pores or microcracks. The number of pores within a certain aperture interval (r_x, r_y) in the soil is M, the aperture r_x corresponds to the

FIGURE 3
Nuclear magnetic resonance instrument.

FIGURE 4
Water retention and morphology of the sample were fixed.

FIGURE 5
Soil sample saturation.

aperture distribution ratio η_x, and r_y corresponds to the aperture distribution ratio η_y, then M can be expressed as:

$$M = \frac{(\eta_x + \eta_y)(r_y - r_x)}{2} \tag{2}$$

Where M_0 represents the total number of pores in the micropore segment at a resting age of 0d, M_t represents the total number of pores in the micropore segment of resting t, and M_u represents the total number of pores in the micropore segment of undisturbed soil. As the resting ages increases, the degree of change in the number of pore in micropore segments can be expressed by the thixotropic conversion ratio D:

$$D = \frac{M_t}{M_0} \tag{3}$$

As the resting ages increases, compared with the undisturbed soil, the degree of change in the number of pore of micropore segments can be expressed by the thixotropic conversion recovery ratio E:

$$E = \frac{M_u - M_0}{M_t - M_0} \tag{4}$$

Set the number of nuclear magnetic test points in the micropore segment to l, corresponding to the aperture distribution ratio η_1, η_2, η_3 to η_l, The thixotropic conversion ratio D can be calculated as:

$$D = \frac{M_t}{M_0} = \frac{\sum_{i=1}^{l}\left(\frac{(\eta_{i,t} + \eta_{i+1,t})(r_{i+1} - r_i)}{2}\right)}{\sum_{i=1}^{l}\left(\frac{(\eta_{i,0} + \eta_{i+1,0})(r_{i+1} - r_i)}{2}\right)} = \sum_{i=0}^{l}\left(\frac{\eta_{i,t} + \eta_{i+1,t}}{\eta_{i,0} + \eta_{i+1,0}}\right) \tag{5}$$

The thixotropic conversion recovery ratio E is:

$$E = \frac{M_u - M_0}{M_t - M_0}$$

$$= \frac{\sum_{i=1}^{l}\left(\frac{(\eta_{i,u} + \eta_{i+1,u})(r_{i+1} - r_i) - (\eta_{i,0} + \eta_{i+1,0})(r_{i+1} - r_i)}{2}\right)}{\sum_{i=1}^{l}\left(\frac{(\eta_{i,t} + \eta_{i+1,t})(r_{i+1} - r_i) - (\eta_{i,0} + \eta_{i+1,0})(r_{i+1} - r_i)}{2}\right)}$$

$$= \sum_{i=1}^{l}\left(\frac{(\eta_{i,u} + \eta_{i+1,u}) - (\eta_{i,0} + \eta_{i+1,0})}{(\eta_{i,t} + \eta_{i+1,t}) - (\eta_{i,0} + \eta_{i+1,0})}\right) \tag{6}$$

In the mesopore and macropore, the D and E are calculated in the same way as in the micropores.

3.2.3 Analysis of aperture distribution ratio curve

Figure 12 depicts the relationship between aperture and aperture distribution ratio, obtained from Equation (1). The graph displays two peaks from left to right, representing micropores and macropores, respectively. The peak size of micropores in both undisturbed and remolded loess is around 1–2 μm. When the particle size varies in the interval of 0–7 μm and 200–4000 μm, the proportion of undisturbed loess is larger than that of remolded loess. However, in the interval of 7–200 μm, the distribution proportion of undisturbed loess is smaller than that of remolded loess.

The results demonstrate that as the resting ages increases, the proportion of peak micropores in the remolded loess continuously
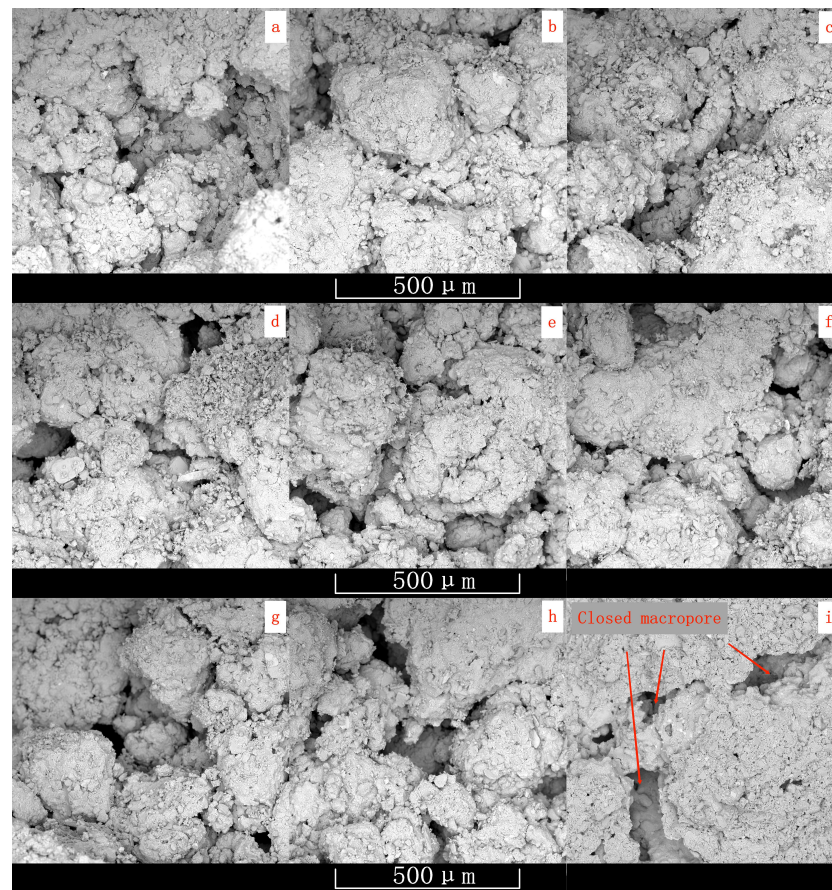
FIGURE 6
Electron microscopic image of undisturbed soil and remodeled soil of different resting ages (**A–I**, ×300).

increases. Compared with that in the remolded loess, the proportion of peak micropores in the remolded loess increased from 0.299% to 0.34%. The nuclear magnetic resonance test point data of 0–7 µm micropore segment was brought into Equation (5) to calculate, and the thixotropic conversion ratio of the aperture representing a 13.9% increment. It is worth noting that the pores at this size are cemented pores, indicating that as the resting ages increases, disturbed clay particles in the soil gradually transit from the dispersed state to cemented state. Consequently, the proportion of cemented pores increases.

Figure 12 reveals that there are no new pore peaks within the undisturbed and remolded loess in the interval of 2–400 µm. In this section, clay particles are filled in the inlay pores of coarse particles or the incohesive micro-cracks between small aggregates to varying degrees. As the aperture increases, the aperture distribution ratio ranging from 2–400 µm indicates a unidirectional downward trend, and no pore peak appears at a certain scale.

Figure 12 reveals that as the resting ages increases, the aperture distribution ratio in the interval of 0–7 µm in the remolded loess increases. This may be attributed to the accumulation of free cements in the coarse-grained mosaic pores so the number of mosaic pores above 7 µm partially reduces. On the other hand, the number of pores smaller than 7 µm increases. Figure 11 also indicates that the pore proportion of 7–400 µm decreases

continuously, and the aperture distribution ratio of about 20 µm changes significantly. The nuclear magnetic resonance test point data of 7–400 µm mesopore segment was brought into Equation (5) to calculate, and the thixotropic conversion ratio of the aperture representing an decrement of 14.4%. This increment primarily originates from the accumulation of free cements or the internal adjustment of the soil structure in the pore section, which reduces the number of large micro-cracks between or within the aggregates. These results can also be observed in SEM images with different resting ages and magnifications of 500 and 1000 times.

The aperture interval of macropore in the undisturbed loess and remolded loess are concentrated between 400 and 3000 µm. This interval is a through microcrack caused by the aeration of large aggregates in the soil. The peak of aperture distribution proportion of macropores in the remolded loess increased from 0.0179% to 0.0183% at a resting age of 160d compared with 0d. The nuclear magnetic resonance test point data of 400–4000 µm macropore segment was brought into Equation (5) to calculate, and the thixotropic conversion ratio of the aperture representing an increment of 2.3%. Due to the difficulty of filling macropores with a limited content of cement, the proportion change may be caused by the shape change of large aggregates during thixotropic process.

An analysis was conducted on the aperture distribution in different size segments of undisturbed and remolded loess at
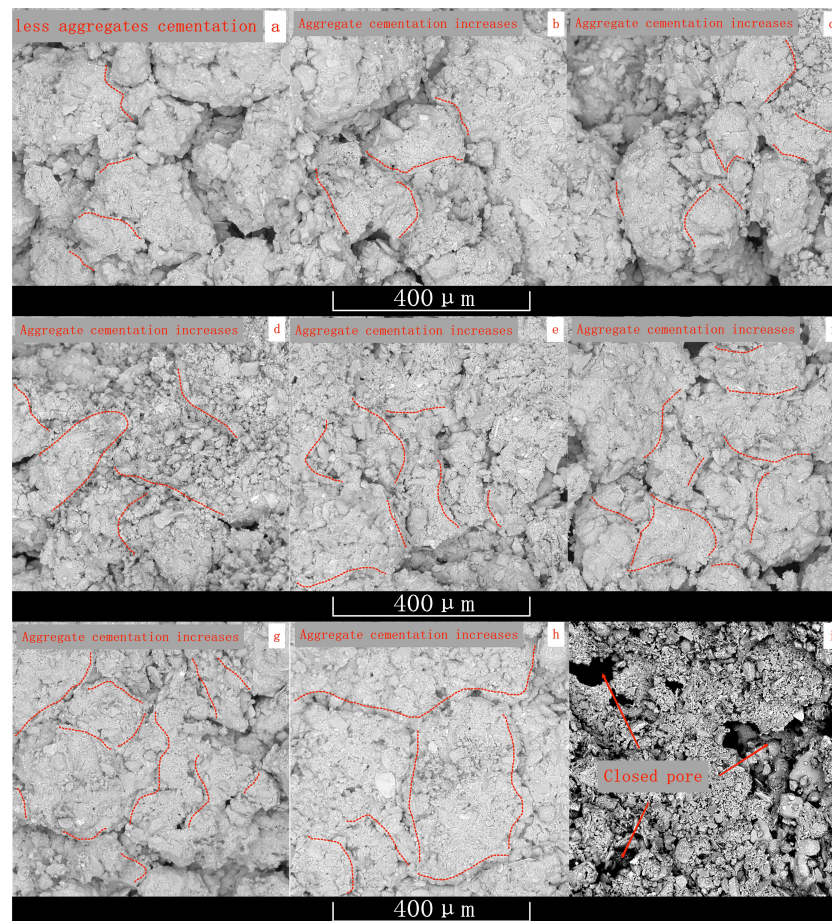
FIGURE 7
Electron microscopic image of undisturbed soil and remolded soil of different resting ages (**A–I**, ×500).

various resting ages. The results indicated that the proportion of micropores is 0.377% in the undisturbed loess, which is 0.078% higher than that in the remolded loess at a resting age of 0d and is 0.037% higher than that in the remolded loess at a resting age of 160d. According to Equation (6), the thixotropic conversion recovery ratio of micropores in the remolded loess at a resting age of 160d is 53.2%.

Figure 12 reveals that the proportion of mesopores with an approximate size of 20 μm changed significantly and the proportion of undisturbed loess was 0.141%, which is 0.074% lower than that of remolded loess at a resting age of 0d. According to Equation (6), the thixotropic conversion recovery ratio of mesopores in the remolded loess at a resting age of 160d is 76.0%.

Finally, Figure 12 demonstrates that the aperture distribution ratio of the peak value of macropores in the undisturbed loess is 0.065%, which is 0.0472% higher than that of the remolded loess at a resting age of 0d and is 0.0468% higher than that of the remolded loess at a resting age of 160d. According to Equation (6), the thixotropic conversion recovery ratio of macropores in the remolded loess at a resting age of 160d is only 0.87%.

The performed analyses demonstrate that part of the evolution from remolded to undisturbed loess is that the proportion of micropores (0–7 μm) and macropores (400–4000 μm) increases,

while the proportion of mesopores (7–400 μm) decreases. This may be attributed to the thixotropic process in which the number of cemented pores increases, while the number of aggregate micro-cracks decreases during the resting period of the remolded loess. However, the number of macropores (400–4000 μm) in the remolded loess does not increase significantly in a short time.

4 Analysis of the thixotropic micromechanical mechanism of loess

4.1 Relationship between soil particle interaction and mesostructural changes

The interactions between soil particles are complex, and the interaction between clay particles, water, and the charge system is one of the most common interactions. This interaction involves both attraction and repulsion forces, which contribute to cohesion observed in the attraction and repulsion between soil particles. The attraction between clay particles involves various forces, including electrostatic attraction, van der Waals force, interparticle cementation, and contact point bonding. Electrostatic attraction consists of Coulomb force and ion electrostatic force. Clay particles,
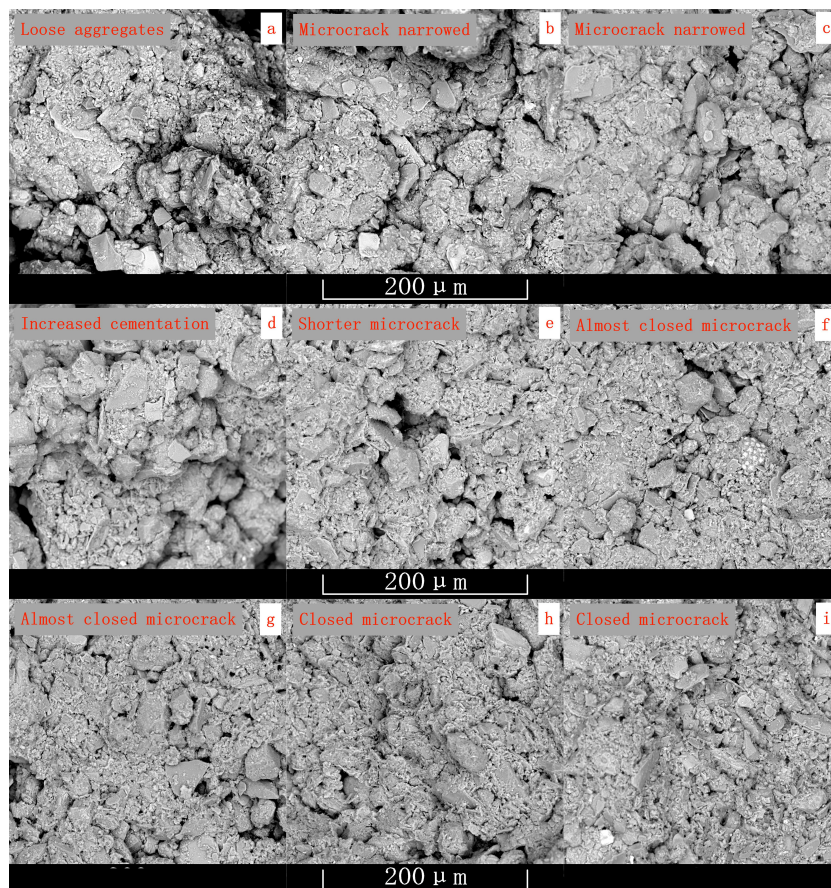
FIGURE 8
Electron microscopic image of undisturbed soil and remodeled soil of different resting ages (**A–I**, ×1000).

which are typically in a sheet form, carry a negative charge on plane and edge regions. The Coulomb force induces positive and negative charges on clay particles to be attracted by face–edge contact. Moreover, the ionic electrostatic force results in the absorption of negatively-charged clay particles by cations in pore water. This

overlapping of double electric layers forms a common water film and attraction. When two polar molecules approach each other, one of the polar molecules will attract the opposite dipole. The cementation between clay particles comes from chemical reactions, including the interaction between clay particles (such as
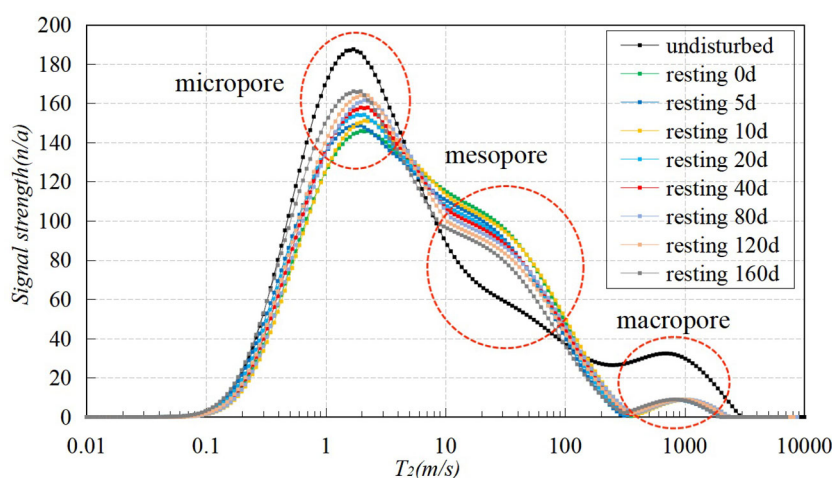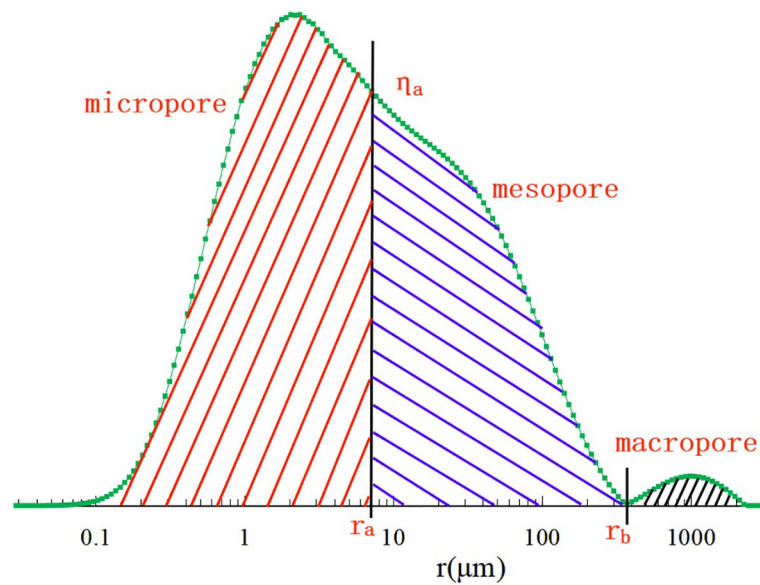

FIGURE 9
Signal strength–T2.

FIGURE 10
Aperture partition diagram (a).

illite, montmorillonite, and kaolinite) and free oxides, organic matter, salt solution, and even coarse particles in the soil. Therefore, clay particles in the soil can be consolidated into clusters, or the coarse particles and detritus particles wrapped in minerals, forming large flocculation structures. Contact point bonding primarily originates from the deformation and compression of load, which reduces the contact distance of mineral particles and produces high-energy bonding.

The soil is compressed and deformed under the action of external loads. On the other hand, the shape and position of the soil particles change as the contact area between the soil particles increases. Consequently, the connection to the original structure breaks, the distribution of the pore water solution changes, and the removal of detrital particles, including detrital minerals and clay

particles, becomes more pronounced. Structural changes reflect the work done by external forces. When the soil is compressed and its volume remains constant, a portion of the compressive elastic deformation generated by soil particles is transformed into consolidation contact of soil particles, while the other portion cannot overcome the minimum gravitational distance of soil particles. In this case, the resultant force cannot overcome the repulsion between soil particles and transforms into elastic potential energy stored.

When the soil is compressed, clay particles and cationic water solution generated by the compression disturbance are redistributed in the newly formed pores. Furthermore, the clay–water–charge system re-establishes attraction, and more cements appear in the short term to form flocculated aggregates, which is consistent with
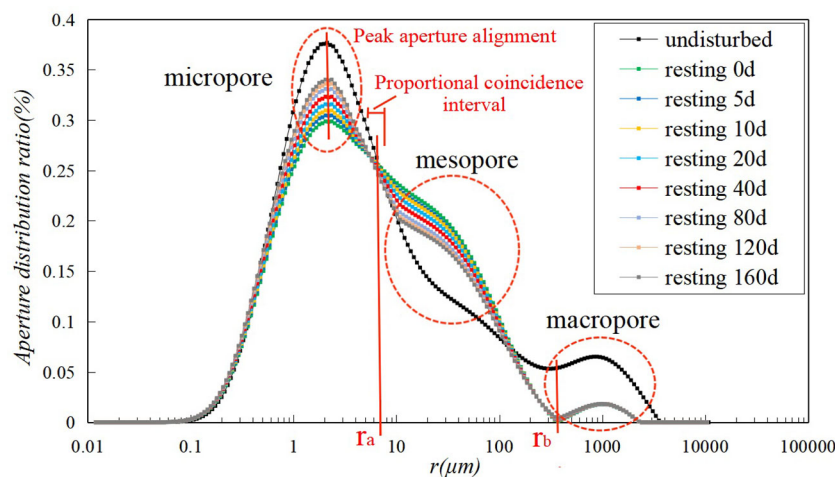

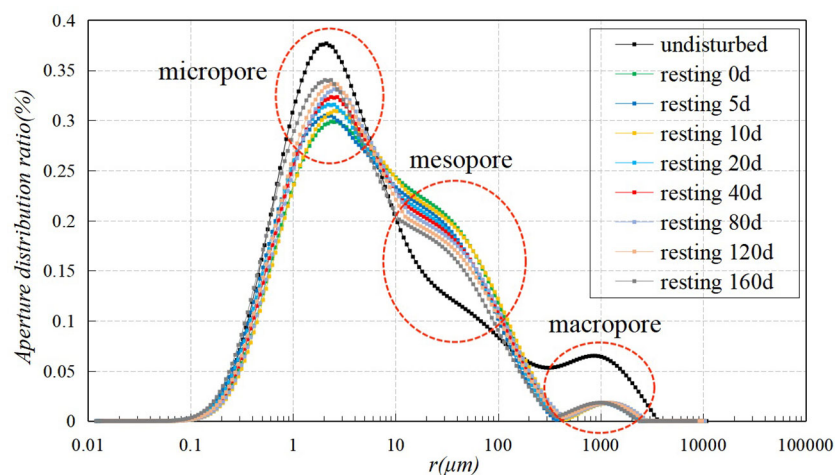**FIGURE 11**
Aperture partition diagram (b).

FIGURE 12
Aperture distribution ratio.

the recently published report indicating that the proportion of clay thixotropic strength in many areas is only positively correlated with cation exchange capacity by Zhang et al. (2017). Meanwhile, the elastic potential energy stored in the soil is gradually released, which may change the shape of clay particles. This phenomenon may result in face–edge attraction under the action of Coulomb force, or change the position of particles. When the average distance between soil particles is relatively small, the cations establish a mutual attraction with the water film. The compression squeezes the saturated aqueous solution in some pores into the external pores, and the aqueous solution is evenly dispersed in the pores in the later resting ages. When the saturated solution contacts with soil particles nearby, they attract each other due to the ionic electrostatic force.

The longer the resting ages, the more energy dissipates in the system, the activity of soil particles weakens, the distribution of pore water becomes more uniform, fewer clay particles form cement, the cation exchange reaction weakens in the aqueous solution, and the strength growth range reduces. The thixotropic process lasts for a long time. This may be attributed to the attraction between clay particles to form cements and the gradual flocculation of aggregates to produce precipitation. This process is related to the number of clay particles involved per unit time and the concentration of cations in water. With the growth of resting ages, the number of clay particles and cation concentration involved in the cementation reaction becomes smaller, and the formation time of flocculation precipitation becomes longer. Therefore, the processing time of thixotropic strength growth is especially long.

4.2 Relationship between microstructural changes of loess and growth of thixotropic strength

During the experiment, external forces were applied to the soil to produce shear failure. The failure surface typically occurs in the area with weak cementation and small cementation areas, which are often more extended. It may also occur through cracks. In order to improve the structural strength of soil, consolidation, and compaction techniques were initially applied to reduce initial pores. Consequently, the cementation area of soil particles increased and the shear strength of the failure surface enhanced. For a constant volume of soil under the action of the clay–water–charge system, newly generated thixotropic cements increase the cementation area between soil particles or increase the friction force. This process can be primarily categorized into four forms: wide crack uncontacted, crack convex occlusal contact, narrow crack contact, and slightly convex occlusal contact.

Figures 13A, B show the non-contact form of wide cracks. Due to the large width of the micro-crack, the content of newly generated cements attached to both sides of the aggregate decreases after the soil thixotropy. Consequently, a crack with a large width may not close completely and its ability to resist shear force becomes limited. As a result, the structural strength cannot be improved.

Figures 13C, D show the occlusal contact form with the fissure protuberance. The raised soil particles on both sides of the microcracks are in contact with each other, providing a certain resistance to shear forces. However, if the raised soil particles contain microcracks, they are prone to peel off and failure under stress. During the thixotropic process, the formation of cement enhances the closure of microcracks at the bulge, preventing the removal of raised soil particles, thereby increasing the friction force on the shear failure surface.

Figures 13E, F show the contact form of a narrow crack. soil already has a consolidation cementing surface due to early compression so newly generated cements in the thixotropic process accumulate in the periphery of the original consolidated contact surface. As a result, the consolidated area of the aggregate contact point increases and the cohesion of the shear failure surface improves.

Figures 13G, H illustrate the occlusal contact form of slight raised. It is observed that the raised soil particles on both sides of the
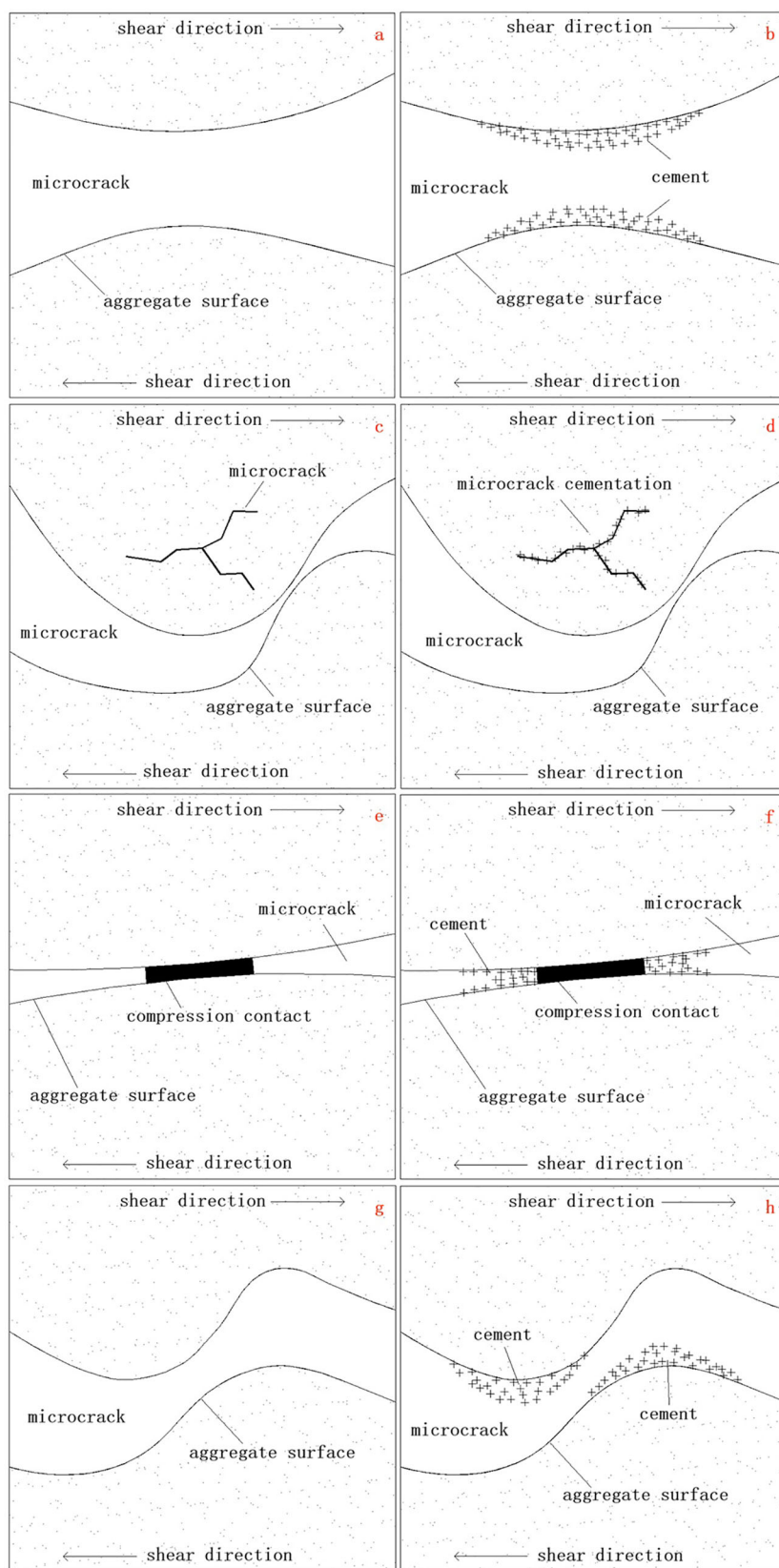
FIGURE 13
Influence of soil structure change on micro-strength before and after thixotropy **(A–H)**.

aggregate in the microcrack are relatively low, and the occlusal shear resistance is small. However, during the thixotropic process, the newly generated cements gather at the uplift, increasing their height and enhancing the shear resistance at the occlusal contact, thereby increasing the friction force of the shear failure surface.

5 Conclusion

In the present study, thixotropic mechanism of loess was investigated. The performed analyses revealed that Xi'an loess exhibits pronounced thixotropy. SEM photos of the remolded loess and undisturbed loess at different magnifications indicate that undisturbed loess contains closed macropores larger than 500 μm, as well as inlaid pores between soil particles ranging from 10–40 μm. In contrast, it is found that there is no microcrack with small aggregates. The remolded loess contained 700 μm macropores in the aggregate frame, 100–300 μm small aggregate microcracks, and 10–40 μm inlay pores among soil particles. The results demonstrate that as the resting ages increases, the cementation and closure of 100–300 μm microcracks shrink gradually, which improves the cohesion and friction between aggregates to a certain extent. This finding is of significant importance to improve the thixotropic strength of the remolded loess.

NMR results indicated that the proportions of micropores (0–7 μm) and macropores (200–4000 μm) in the undisturbed loess are higher than those in the remolded loess at different resting ages. Moreover, it is found that the proportion of mesopore (7–200 μm) is lower than those in the remolded loess at different resting ages. The proportion of micropores in the interval of 1–2 μm in the reconstituted loess increased with the increase of the resting ages. At a resting age of 160d, the thixotropic conversion ratio D and thixotropic conversion recovery ratio E of remolded loess with micropores are 13.9% and 53.2%, respectively. The thixotropic conversion ratio D and thixotropic conversion recovery ratio E of remolded loess with mesopores are 14.4% and 76.0%, respectively. The thixotropic conversion ratio D and thixotropic conversion recovery ratio E of remolded loess with macropores are 2.3% and 0.8%, respectively. A portion of the evolution process from remolded to undisturbed loess is the thixotropic behavior of increasing the number of cemented pores and decreasing the number of aggregate microcracks.

The increase in the thixotropic strength in loess can be attributed to the micromechanical mechanism described as follows: when the soil is resting, the interaction between soil particles and aqueous solution re-establishes attractive forces within the disturbed clay particle–water–charge system. Consequently, more clay cements are absorbed in the microcracks of aggregates in a short time. Simultaneously, the elastic potential energy induced by compression weakens due to partial deformation and displacement of soil particles during resting storage. Moreover, the migration of pore water and some clay particles promotes the mutual cementation of dispersed clay particles. The cementation area and the occlusal degree of soil particles at the meso level increased, which enhanced the structural strength at the macro level. However, the cation content of clay particles and water solution in the system is limited and is constantly consumed in the thixotropic process due to the formation of cements. The expansion of cements takes a longer time to form flocculant precipitation so the proportion of strength increasing with the resting ages decreases continuously.

Data availability statement

The original contributions presented in the study are included in the article/Supplementary material. Further inquiries can be directed to the corresponding authors.

Author contributions

All authors listed have made a substantial, direct, and intellectual contribution to the work and approved it for publication.

Conflict of interest

The authors declare that the research was conducted in the absence of any commercial or financial relationships that could be construed as a potential conflict of interest.

Publisher's note

All claims expressed in this article are solely those of the authors and do not necessarily represent those of their affiliated organizations, or those of the publisher, the editors and the reviewers. Any product that may be evaluated in this article, or claim that may be made by its manufacturer, is not guaranteed or endorsed by the publisher.

References

Abdou, M. I., and Ahmed, H. E. S. (2013). A study on the thixotropy of Egyptian bentonite suspensions. *Pet. Sci. Technol.* 31 (19), 1980–1991. doi: 10.1080/10916466.2011.554060

Abu-Farsakh, M., Rosti, F., and Souri, A. (2015). Evaluating pile installation and subsequent thixotropic and consolidation effects on setup by numerical simulation for full-scale pile load tests. *Can. Geotech. J.* 52 (11), 1734–1746. doi: 10.1139/cgj-2014-0470

Aminpour, P. (2019). *Multiscale modeling of thixotropy in soft clays*. (Philadelphia, PA: Drexel University).

Andersen, K. H., Lunne, T., Kvalstad, T. J., and Forsberg, C. F. (2008). "Deep water geotechnical engineering," in *Proc. 24th Nat. Conf. of Mexican Soc. of Soil Mechanics*. 26–29. (Aguasclientes, Mexico).

Barnes, H. A. (1997). Thixotropy—a review. *J. Non-Newtonian Fluid Mech.* 70 (1–2), 1–33. doi: 10.1016/S0377-0257(97)00004-9

Blake, G. R., and Gilman, R. D. (1970). Thixotropic changes with aging of synthetic soil aggregates. *Soil Sci. Soc Am. J.* 34 (4), 561–564. doi: 10.2136/sssaj1970.03615995003400040009x

Boswell, P. G. H. (1948). A preliminary examination of the thixotropy of some sedimentary rocks. *Q. J. Geol. Soc* 104 (1–4), 499–526. doi: 10.1144/GSL.JGS.1948.104.01-04.23

Burgers, J. M., and Blair, G. W. S. (1949). *Report on the principles of rheological nomenclature* (Netherlands: North-Holland Publishing Company. International Council of Scientific Unions. Joint Committee on Rheology).

Day, P. R., and Ripple, C. D. (1954). Effect of shear on suction in saturated clays. *Annual Reports I and II, Western Regional Research Project W-30*, 1955, 675-679. doi: 10.2136/sssaj1966.03615995003600060010x

de Souza Mendes, P. R. (2009). Modeling the thixotropic behavior of structured fluids. *J. Non-Newtonian Fluid Mech.* 164 (1–3), 66–75. doi: 10.1016/j.jnnfm.2009.08.005

Dexter, A. R., Horn, R., and Kemper, W. D. (1988). Two mechanisms for age-hardening of soil. *J. Soil Sci.* 39 (2), 163–175. doi: 10.1111/j.1365-2389.1988.tb01203.x

Díaz-Rodríguez, J. A., and Santamarina, J. C. (1999). "Thixotropy: the case of Mexico city soils," in *XI Panamerican Conf. on Soil Mech. and Geotech. Eng.* 441–448. (Brazil).

Doglioni, A., and Simeone, V. (2013). "Recovery of strength along shear surfaces in clay soils," in *Landslide Science and Practice* (Berlin, Heidelberg: Springer), 183–188.

Dullaert, K., and Mewis, J. (2006). A structural kinetics model for thixotropy. *J. NonNewtonian Fluid Mech.* 139 (1–2), 21–30. doi: 10.1016/j.jnnfm.2006.06.002

Gagnoud, M., Lajeunesse, P., Desrosiers, G., Long, B., and Stora, G. (2008). Litho- and biofacies analysis of postglacial marine mud using CT-scanning. *Eng. Geol.* 103 (3), 106–111. doi: 10.1016/j.enggeo.2008.06.010

Heymann, L., Noack, E., Kämpfe, L., and Beckmann, B. (1996). "Rheology of printing inks—some new experimental results," in *Proceedings of the XIIth Congress on Rheology*. Ed. Ait-Kadi, JM James and MC Williams. (Quebec, Canada: Laval University), 451–452.

Jacobsson, A., and Pusch, R. (1972). Thixotropic action in remoulded quick clay. *Bull. Int. Assoc. Eng. Geology-Bulletin l'Association Internationale Géologie l'Ingénieur* 5 (1), 105–110. doi: 10.1007/BF02634659

Jeong, S. W., Locat, J., and Leroueil, S. (2012). The effects of salinity and shear history on the rheological characteristics of illite-rich and Na-montmorillonite-rich clays. *Clay Clay Miner.* 60 (2), 108–120. doi: 10.1346/CCMN.2012.0600202

Jiang, H., Mu, J., Zhang, J., Jiang, Y., Liu, C., and Zhang, X. (2022). Dynamic evolution in mechanical characteristics of complex supporting structures during large section tunnel construction. *Deep Underground Sci. Eng.* 1 (2), 183–201. doi: 10.1002/dug2.12027

Liu, J., Xue, Y., Fu, Y., Yao, K., and Liu, J. (2023). Numerical investigation on microwave-thermal recovery of shale gas based on a fully coupled electromagnetic, heat transfer, and multiphase flow model. *Energy* 263, 126090. doi: 10.1016/j.energy.2022.126090

Lu, N. Z., Suhayda, J. N., Prior, D. B., Bornhold, B. D., Keller, G. H., Wiseman, W. J., et al. (1991). Sediment thixotropy and submarine mass movement, Huanghe Delta, China. *Geo-Mar. Lett.* 11 (1), 9–15. doi: 10.1007/BF02431049

Mitchell, J. K. (1961). Fundamental aspects of thixotropy in soils. *Trans. Am. Soc Civ. Eng.* 126 (1), 1586–1620. doi: 10.1061/TACEAT.0008103

Olphen, H. V. (1977). An introduction to clay colloid chemistry. *Soil Science*, 97 (4), 290. (USA).

Osipov, V. I., Nikolaeva, S. K., and Sokolov, V. N. (1984). Microstructural changes associated with thixotropic phenomena in clay soils. *Geotechnique* 34 (3), 293–303. doi: 10.1680/geot.1984.34.3.293

Pardo, G. S., Sarmah, A. K., and Orense, R. P. (2019). Mechanism of improvement of biochar on shear strength and liquefaction resistance of sand. *Geotechnique* 69 (6), 471–480. doi: 10.1680/jgeot.17.P.040

Perret, D., Locat, J., and Martignoni, P. (1996). Thixotropic behavior during shear of a finegrained mud from Eastern Canada. *Eng. Geol.* 43 (1), 31–44. doi: 10.1016/0013-7952(96)00031-2

Peterfi, T. (1927). Die abhebung der befruchtungsmembran bei seeigeleiern: Eine kolloidchemische Analyse des Befruchtungsvorganges. *Wilhelm Roux'Archiv für Entwicklungsmechanik der Organismen* 112, 660–695. doi: 10.1007/BF02253780

Rinaldi, V. A., and Clariá, J. J. J. (2016). Time dependent stress–strain behavior of bentonite slurries; effect of thixotropy. *Powder Technol.* 291, 311–321. doi: 10.1016/j.powtec.2015.12.036

Shahriar, A. R., Abedin, M. Z., and Jadid, R. (2018). Thixotropic aging and its effect on 1-D compression behavior of soft reconstituted clays. *Appl. Clay Sci.* 153, 217–227. doi: 10.1016/j.clay.2017.12.029

Skempton, A. W., and Northey, R. D. (1952). The sensitivity of clays. *Geotechnique* 3 (1), 30–53. doi: 10.1680/geot.1952.3.1.30

Sun, X., Li, X., Zheng, B., He, J., and Mao, T. (2020). Study on the progressive fracturing in soil and rock mixture under uniaxial compression conditions by CT scanning. *Eng. Geol.* 279, 105884. doi: 10.1016/j.enggeo.2020.105884

Sun, H., Masin, D., Najser, J., Nedela, V., and Navratilova, E. (2019). Bentonite microstructure and saturation evolution in wetting-drying cycles evaluated using ESEM, MIP and WRC measurements. *Géotechnique* 69 (8), 713–726. doi: 10.1680/jgeot.17.P.253

Xue, Y., Liu, S., Chai, J., Liu, J., Ranjith, P. G., Cai, C., et al. (2023b). Effect of water-cooling shock on fracture initiation and morphology of high-temperature granite: Application of hydraulic fracturing to enhanced geothermal systems. *Appl. Energy* 337, 120858. doi: 10.1016/j.apenergy.2023.120858

Xue, Y., Liu, J., Liang, X., Li, X., Wang, S., Ma, Z., et al. (2023a). Influence mechanism of brine-gas two-phase flow on sealing property of anisotropic caprock for hydrogen and carbon energy underground storage. *Int. J. Hydrogen Energy* 48 (30), 11287–11302. doi: 10.1016/j.ijhydene.2022.05.173

Xue, Y., Ranjith, P. G., Gao, F., Zhang, Z., and Wang, S. (2023c). Experimental investigations on effects of gas pressure on mechanical behaviors and failure characteristic of coals. *J. Rock Mechanics Geotechnical Eng.* 15 (2), 412–428. doi: 10.1016/j.jrmge.2022.05.013

Yang, Z., Qi, W., Ding, Y., Jiang, Y., Yang, X., Yang, X., et al. (2023). Numerical investigation on the spewing mechanism of earth pressure balance shield in a high-pressure water-rich sand stratum. *Deep Underground Sci. Eng.* 2 (1), 74–87. doi: 10.1002/dug2.12032

Zhang, X. W., Kong, L. W., Yang, A. W., and Sayem, H. M. (2017). Thixotropic mechanism of clay: a microstructural investigation. *Soils Found.* 57 (1), 23–35. doi: 10.1016/j.sandf.2017.01.002